Transitional Behavior of MPD Arcjet Operation

Kyoichi Kuriki* and Hiroshi Suzuki†
Institute of Space and Aeronautical Science
University of Tokyo, Komaba, Meguro-ku, Tokyo, Japan

The thrust and discharge voltage of a quasisteady MPD arcjet have been measured, with emphasis on the transitional characteristics from the propellant over-fed to starved condition and from aerodynamic to electromagnetic acceleration. From the anode and cathode potential measurements, the transition into the starved condition was found to be preceded slightly by the transition of acceleration process when the discharge current was increased. At the beginning of the electromagnetic acceleration, the thrust became unstable. This was attributable to radial current expansion toward the outer anode region. At higher discharge current, the flow pattern settled and the quasisteady state was restored.

I. Introduction

THE improvement of MPD arcjet performance has been achieved by increasing the input power for a fixed mass flow rate $\dot{m}$. This policy requires an increase in the fractional power invested in the electromagnetic acceleration. Efforts along this line have confronted difficulties in that the arcjet operation began to be erratic and inefficient at a certain limit of the input power or discharge current J. The key parameter was found to be $J^2/\dot{m}$ from the voltage fluctuation measurement,[1] and the exhaust speed was found to be limited below a certain level.[1,2] Anomalies are also found in the anode heat transfer as a sudden enhancement with the discharge current,[2] and in the voltage-current characteristics as a change in the functional form of J.[4] The critical value of $J^2/\dot{m}$ was analytically derived from the rule of minimum input power[1] or drift speed approximation[5] based on the idea of burning voltage.[6] The anomalous features mentioned above were observed more or less near the predicted $(J^2/\dot{m})_{cr}$. No physical basis, however, has yet been successfully given to relate definitely the predicted $(J^2/\dot{m})_{cr}$ to the observed anomalies.[7]

It has been recognized as a common feature among experiments[1-5] that the mass starved condition, i.e., the current carrier shortage, is reached by increasing the discharge current for a fixed mass flow rate. The discharge is forced to self-adjust the carrier shortage by either 1) entraining the materials from the eroded electrode or insulator, the outgas from the heated wall, and the preinjected mass around the discharge region; 2) accelerating the electrons by the intensified electric field near the anode; or 3) both 1 and 2. The first adjustment is considered to result in the change in the discharge mode, and the second in the enhanced anode loss. It is dependent on the electrode configuration as well as the scheme of gas injection, a phenomenon that is dominant in the starved condition.

The purpose of the present experiment is to find what anomalies appear in the thrust-current and voltage-current characteristics at and beyond the critical condition, and in what manner the starved state is relaxed or continued. A conventional configuration of a quasisteady MPD arcjet was tested in order to compare the results with those of the preceding experiments.[1-4] Anode configuration and gas injection were modified to find their influences in the transitional conditions. The thrust and voltage measurements were supplemented by the diagnostic measurements of Langmuir and magnetic probes.

II. Experimental Apparatus

The cross section of the discharge chamber is shown in Fig. 1. The copper anode and tungsten cathode were separated by an insulator lined with boron nitride. The accelerometer for the thrust measurement was mounted on the back of the cathode base plate. Three discharge chamber configurations were used in this experiment. The first one has gas injection ports at the middle between electrodes, as shown in Fig. 2a, and is called midpoint gas injection (MI). The second has two ports at the middle and two others near the anode surface, as shown in Fig. 2b, and is called surface gas injection (SI). With this configuration, the propellant-starved condition was expected to be improved as observed in Ref. 4. In the present experiment, some data for MI and SI showed little difference and were described without specifying the type as MI or SI. The third has a plastic (acetal copolymer) anode hood as shown in Fig. 2c. The original intention of using the hood was to prevent the spontaneous breakdown that occurred at extremely large current and small mass flow rate between anode and cathode back plate or cable terminal if incompletely covered by the insulator. In the course of the experiment, however, the results for this configuration were found to be informative, as will be discussed later. For free displacement, the discharge chamber was suspended in a vacuum tank by nylon strings as shown in Fig. 1. The discharge chamber was also tied to the side surface of the tank by other nylon strings with just enough tension to restrict sideway movement. Since the axial displacement of the discharge chamber during 1 ms operation was less than 20 μm, the thrust was measured in an almost resistance-free condition. The working gas was introduced into the annular electrode gap through rubber tubings that were flexible enough to assure little resistance against the chamber displacement. The vacuum tank was 1.5 m in diameter and 2.8 m long. The pressure inside the tank was less than 10^{-3} Pa before each run, and less than 10^{-2} Pa just after the shot. The accelerometer was a PCB 302A06 piezoelectric transducer, which had a flat frequency response up to 10 kHz and a resonant frequency of 45 kHz. In order to eliminate the resonant characteristics, the output signal was processed with a 10-kHz low-pass filter. The responsivity of the accelerometer integrated in the arcjet system, which includes the elasticity and weight of power cables, gas tubings,

Presented as Paper 76-1002 at the AIAA International Electric Propulsion Conference, Key Biscayne, Fla., Nov. 14-17, 1976; submitted Feb. 2, 1978; revision received July 5, 1978.

Index categories: Electric and Advanced Space Propulsion; Plasma Dynamics and MHD.

*Associate Professor, Institute of Space and Aeronautical Science. Member AIAA.

†Graduate Student, Institute of Space and Aeronautical Science.

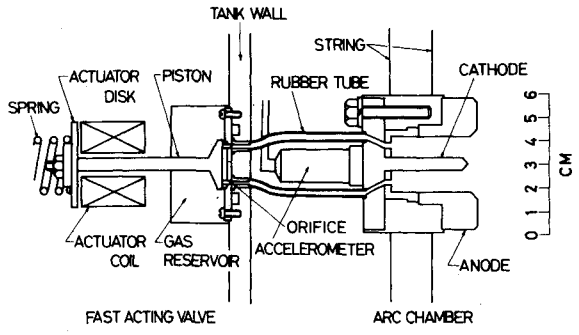

Fig. 1 Schematic of quasisteady MPD arcjet with coaxial electrodes and fast-acting valve.

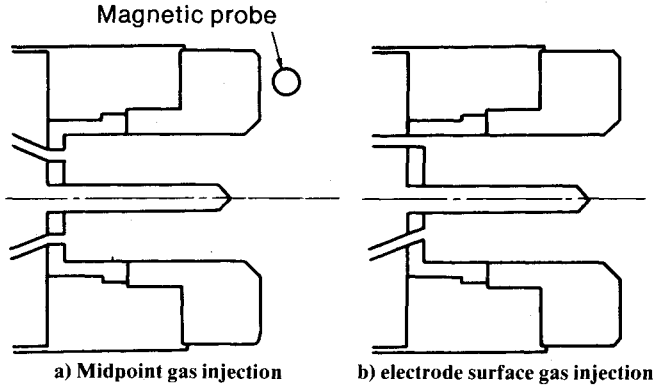

a) Midpoint gas injection **b) electrode surface gas injection**

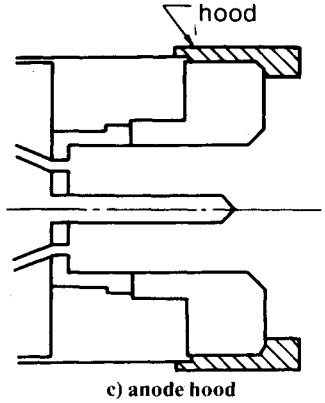

c) anode hood

Fig. 2 Configurations of discharge chamber.

and suspending strings, was calibrated by applying an impulse of known strength in the atmospheric background. The result agreed well with the responsivity of the manufacturer's data above 1 N thrust in this experiment.

The fast-acting valve (FAV) shown in Fig. 1 was used for quasisteady gas injection into the discharge chamber. By energizing the actuator coil, the poppet valve is repelled from the rubber seat against the spring compressional force. The mass flow rate $\dot{m}$ was determined by the choked condition of the orifice flow. The poppet valve was hollowed in order to have a short rise time of the mass flow rate. The gas flow without arc discharge was studied at the arcjet muzzle by a fast ionization gage.[8] The mass flow rate attains a steady value with a 400-μs rise time.[9] The quasisteady $\dot{m}$ duration can be adjusted by the coil current and the spring precompression. The working gases were hydrogen, helium, and argon.

The power supply was a 2,000 μF and 5 kV oil-paper capacitor bank constructing a pulse-forming network (PFN) of 1 ms pulse width. The PFN can supply a single current pulse by a matched resistance in series with the arc discharge. The arc discharge was initiated with a variable time delay with

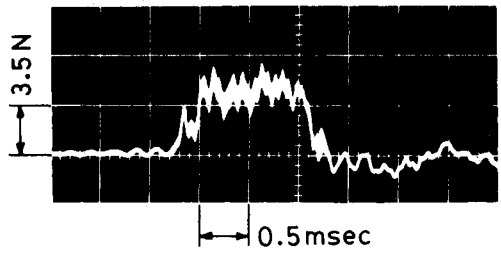

Fig. 3 Accelerometer signal. $J = 5.7$ kA, $\dot{m} = 0.052$ g/s, hydrogen.

reference to the gas pulse. A charging voltage greater than 2 kV appeared between electrodes only after the ignition was turned on, and was large enough to initiate the gas breakdown. As soon as the large current started, most of the voltage drop occurred at the matching resistance, and the arc voltage was a small fraction of the charging voltage. The detailed operational sequence as well as the gas injection studies are described in Ref. 9. The discharge current was measured by a shunt resistance and a calibrated Rogowski coil. For the measurement of the discharge voltage, a current probe was used to monitor the small current bled through a known resistor across the electrodes. The use of the current probe instead of the resistance voltage divider was necessary because the arc discharge circuit, including electrodes, was completely isolated from the tank potential, i.e., the earth potential. The floating discharge system was adopted for two reasons: 1) the spontaneous discharge between the cathode and the tank wall (if the anode is grounded) is easily mixed up with the fluctuating discharge in the starved condition, and 2) in practical cases the discharge current is apt to flow through the spacecraft structure when included in the discharge circuit and is hazardous to the other payloads.

Even when the discharge system was isolated from the earth, the discharge spot would hop around the metal surface explosed to the plasma flow as if it were a "stepping stone." In the case of small mass flow rate and large current, the spot was observed on the tank wall near discharge chamber when its surface was not insulated. Such a metal surface, which is isolated from the power supply but provides a part of current path, is known as a reflector electrode.[10] Thereafter, the metal surfaces near the discharge chamber were totally covered by myler sheet, and the spot was seldom observed.

The self-induced magnetic field B_θ was measured by a magnetic probe of 7-mm diameter and 410 turns. With a suitable terminating resistance and an integrator of 10 ms time constant, the probe has a flat response up to 300 kHz. The radiation from the plasma stream was monitored by a photomultiplier RCA 7102. The output was proportional to the radiation intensity with a weight function of photomutiplier spectral responsivity ranging from 600 nm to 950 nm wavelength.

III. Thrust Measurement

The thrust was measured for the midpoint gas injection (MI) configuration. The typical output signal of the accelerometer is reproduced in Fig. 3. The thrust is almost quasisteady during the 1 ms discharge duration. The measured thrust is plotted against the discharge current in Fig. 4 for argon. The thrust T can be expressed by:

$$T = bJ^2 + \dot{m}u_a \tag{1}$$

$$b = \{\ln(r_a/r_c) + \tfrac{3}{4}\} \times 10^{-7} \text{ (mks units)} \tag{2}$$

where r_a and r_c are the anode and cathode radii, respectively,[11] and u_a is the exhaust speed attained by aerodynamic acceleration converting the thermal energy into the kinetic one. Since the thermal energy is generated by Joule heating, u_a might be proportional to J if the electrical conductivity is

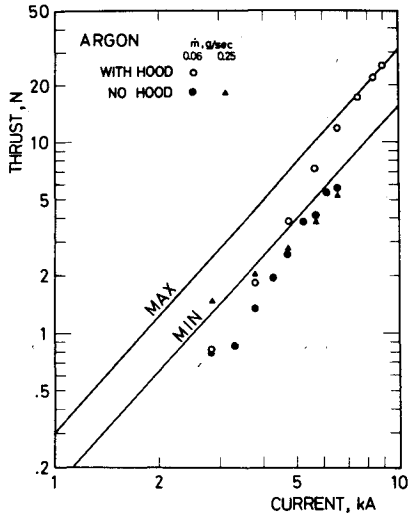

Fig. 4 Thrust-current characteristics with and without anode hood. Solid lines represent theoretical predictions. MAX: $b_{max} = 10^{-7}[\ell n(r_a/r_c) + 3/4]$, $r_a/r_c = 50/5$; MIN: $b_{min} = 10^{-7}[\ell n(r_a/r_c)]$, $r_a/r_c = 24/5$.

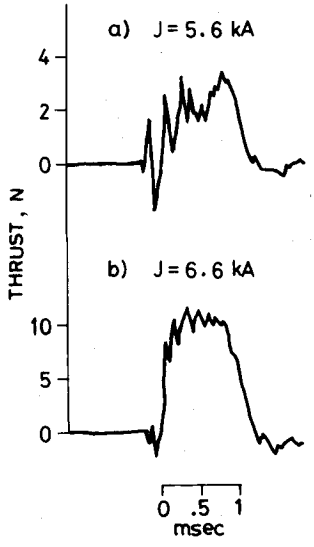

Fig. 5 Accelerometer signals with and without anode hood. $\dot{m} = 0.12$ g/s, argon.

constant. The last assumption will be found to be valid from the voltage-current characteristics shown later. As seen in Fig. 4, at small J and large $\dot{m}$ the aerodynamic acceleration, the second term in Eq. (1), is dominant, and the thrust is proportional to J. At large J or small $\dot{m}$, on the other hand, the electromagnetic acceleration, the first term in Eq. (1), supersedes the other, and the thrust is proportional to J^2. The solid lines marked MAX and MIN in Fig. 4 are the analytical results calculated with the maximum and minimum values of b in Eq. (2), substituting the outer and inner radii of the anode, and including and excluding the term 3/4, respectively. The experimental results are found to be close to the predicted MIN value. A thrust smaller than the prediction at small J might be due to the insufficient accelerometer responsivity below 1 N thrust. The experimental points for no hood in Fig. 4 increase with current more rapidly than J^2 dependence, and approach the MIN line. Above a certain current level, the thrust signal lost the quasisteadiness. However, the thrust signal restored the quasisteady profile at much larger discharge current. These features suggest that the change was not catastrophic, but rather the transition to another discharge mode.

The thrust measured with the anode hood is plotted against the current in Fig. 4 for $\dot{m} = 0.06$ g/s argon, and is compared

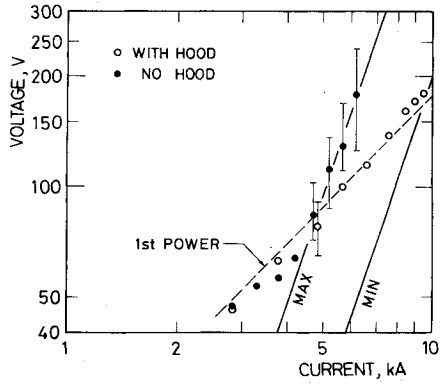

Fig. 6 Voltage-current characteristics with anode hood. $\dot{m} = 0.06$ g/s, argon. MAX and MIN correspond to the same conditions as in Fig. 4.

with the results for the conventional anode. At small J the two results are found to agree quite well. As the current is increased, the plots for the anode hood increase more rapidly than J^2 dependence. Apparently the thrust tends to follow the predicted maximum thrust at large J. The trace of the thrust signal is unsteady in the transitional condition as shown in Fig. 5a, while at large J it restores quasisteadiness as shown in Fig. 5b.

IV. Voltage-Current Characteristics

The voltage-current characteristics are shown in Fig. 6. The discharge voltage of the MPD arcjet is expressed by the sum,[12]

$$V = V_a + V_b + V_c + V_i + V_t \tag{3}$$

where the anode and cathode drops, V_a and V_c, are nearly constant, and $V_a + V_c \simeq 20$ V. V_b is the voltage required for the electromagnetic acceleration and is expressed by

$$V_b = b^2 J^3 / 2\dot{m} \tag{4}$$

V_i and V_t are the voltages required for the ionization and thermalization, respectively, and are given by

$$V_i = e\Phi_i \dot{m}/m_i J \tag{5}$$

and

$$V_t = 3k(T_i + T_e)\dot{m}/2m_i J \tag{6}$$

where Φ_i represents the ionization potential; m_i and T_i the ion mass and temperature, respectively; and T_e the electron temperature. The voltage $V_i + V_t$, the ratio of power dissipated by Joule heating to the discharge current, is proportional to J. It is observed in Fig. 6 that at small J, V is nearly proportional to J, i.e., the conductivity is constant, and the voltage $V_i + V_t$ is considered to be dominant. The constancy of the electrical conductivity can be understood as follows. The electrical conductivity of the arc plasma concerned is described by Spitzer's formula.[13] According to this formula, the electrical conductivity is a weak function of plasma density and is strongly dependent on electron temperature. When the input power is increased and the major power consumption is the ionization, the plasma density increases while the electron temperature increases slowly. These plasma properties imply constant conductivity as long as the current flow pattern is unaffected. At large J, V is found to be proportional to J^3, and V_b might be dominant. V_b was calculated from Eq. (4) for b_{max} and b_{min} and is shown in Fig. 6. As soon as the voltage began to deviate from the linear growth with the current, the voltage signal became unsteady, and far beyond the critical condition the steadiness

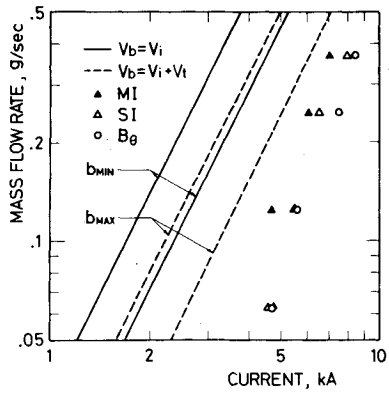

Fig. 7 Critical conditions judged from discharge voltage and B_θ (SI), argon.

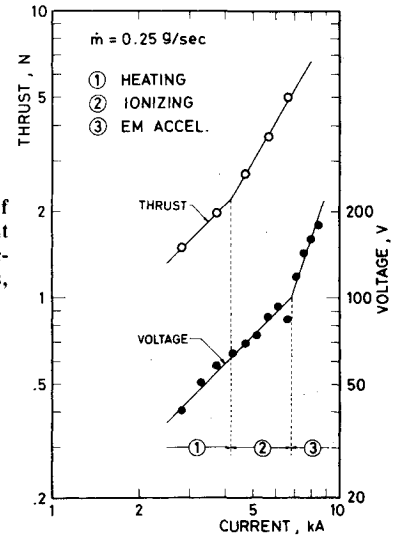

Fig. 8 Comparison of transitions in thrust-current and voltage-current characteristics. $\dot{m}=0.25$ g/s, argon.

was restored. The unsteady signal and rapid increase in voltage were findings similar to those in Refs. 1 and 3, where the enhanced voltage is attributed to the increased anode fall.[3] At the transition of dominant power from the Joule heating power to that required for electromagnetic acceleration, the equation

$$V_b \simeq V_i + V_t \tag{7}$$

holds. Substituting the expression in Eqs. (4-6) into Eq. (7), we get

$$J^2/\dot{m} = u_{tr}/b = \{[2e\Phi_i + 3k(T_i + T_e)]/m_i\}^{1/2}/b$$

where u_{tr} is reduced to $u_{cr} = (2e\Phi_i/m_i)^{1/2}$, i.e., the so-called critical velocity, if the second term in the square bracket is dropped. Near $J^2/\dot{m})_{cr}$ anomalous behavior of the discharge, including anode fall enhancement, was observed in many experiments.[1-4] In the present experiment, the irregularities in the discharge voltage were found to start at $J^2/\dot{m} > J^2/\dot{m})_{tr}$ as shown in Fig. 7, where $T_i = T_e = 4$ eV is assumed with reference to the data in Ref. 9. The experimentally obtained $J^2)_{tr}$ is found to be proportional to $\dot{m}$ in Fig. 7, although its absolute magnitude is slightly greater than the value predicted by Eq. (7) and $b = b_{\max}$. From these considerations, the rapid increase of the discharge voltage with the current can be caused either by the enhanced anode fall or the electromagnetic acceleration, or by both. In order to better understand the rapid voltage rise, the anode and cathode potentials were measured, as will be shown later.

The transitional discharge currents found in thrust-current and voltage-current characteristics are compared in Fig. 8. Apparently, the transition from aerodynamic to electromagnetic thrust occurs at lower current than the transition of major power consumption from Joule heating to electromagnetic acceleration. This difference can be interpreted as follows. When the power input is low, as in the current range labeled 1 in Fig. 8, the power is dissipated in heating the partially ionized plasma and the aerodynamic thrust is dominant. As the current is increased (range 2 in Fig. 8), the input power is spent primarily in ionization. With reference to the enthalpy-temperature relationship of plasma, the temperature does not increase appreciably while the ionization is strongly in progress. This is why the aerodynamic acceleration is no longer promoted and is overridden by the electromagnetic acceleration, whereas the Joule heating is further continued until the plasma is almost fully ionized. In range 3 in Fig. 8, the power is spent mainly in electromagnetically accelerating the almost fully ionized plasma.

The voltage-current characteristics of the hood-attached and conventional anode cases are compared in Fig. 6. With the hood attached, the voltage stays on the linear growth and does not show any abrupt rise at large J, in contrast to the conventional anode. The voltage signal in this case was found to have some irregularities in the same condition as the irregular fluctuation and sudden increases were observed in the conventional anode case. This unsteady behavior is expressed by the bar in Fig. 6, which represents the fluctuation amplitude.

With the results of thrust measurement, the following situations are conceivable. When the discharge is forced to be mass-starved, the discharge mode might be changed into one where more propellant is available. The irregular voltage is considered to reflect the mode transition. At small J the experimental results of the thrust are close to the analytical prediction for $b_{\min}$, which is calculated with r_a equal to the inner anode radius and with the term ¾ ignored. This suggests that the discharge region at small J may be confined in the annular region between anode and cathode and the "blowing force" is dominant. As J increases, the discharge current is considered to spread over the anode front surface, and the experimental points approach the curve for $b_{\max}$, which assumes outer anode radius r_a and the "pumping force" to be effective. For the arc discharge with enlarged anode region, more propellant can be acquired from ablating anode and insulator surfaces. The anode hood exposed to the discharge might be a copious source providing the ablated material and outgas as extra propellants. With these supplementary gases, the ionization and thermalization remain dominant and the voltage exhibits linear growth.

The voltage-current characteristics of surface gas injection are shown in Fig. 9, and compared with those for the midpoint gas injection. The cubic dependence on J as well as the unsteady behavior of the discharge voltage begin at larger current for SI than for MI. Once the critical condition is reached, however, the voltage executes an abrupt rise and becomes as high as in MI case. This characteristic is the intermediate one between those for the conventional and the hood-attached anodes. The propellant utilization for SI might be a little more effective than for MI. Figure 7 shows how experimental $J^2/\dot{m})_{tr}$ is increased in the present case.

As stated in Sec. II, the discharge voltage has been measured by the current probe monitoring the bleeder current. The anode and cathode potentials with respect to the earth were measured to separate the respective electrode phenomena. In Ref. 3, the floating potential of a Langmuir probe was measured with reference to the cathode potential to analyse the correlation between the voltage enhancement and the anode loss. The difference between the floating potential of a Langmuir probe placed in the present plasma flow and the earth potential, i.e., the tank potential, was found to be small compared with the above-mentioned anode and cathode potentials. The reason might be that the plasma flow impingement on the end surface of the tank, as well as the transverse diffusion toward the wall, settles the plasma

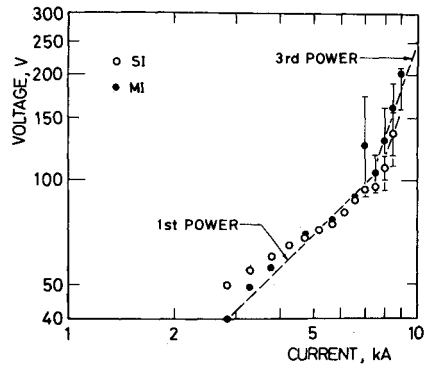

Fig. 9 Voltage-current characteristics for electrode surface gas injection (SI) and midpoint gas injection (MI). $\dot{m} = 0.37$ g/s, argon.

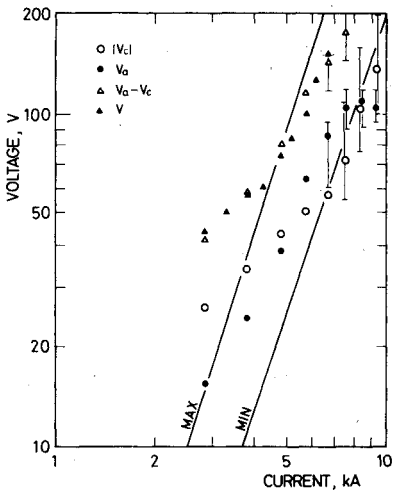

Fig. 10 Anode and cathode potentials and discharge voltage. $\dot{m} = 0.12$ g/s, argon. V_a = anode potential, V_c = cathode potential.

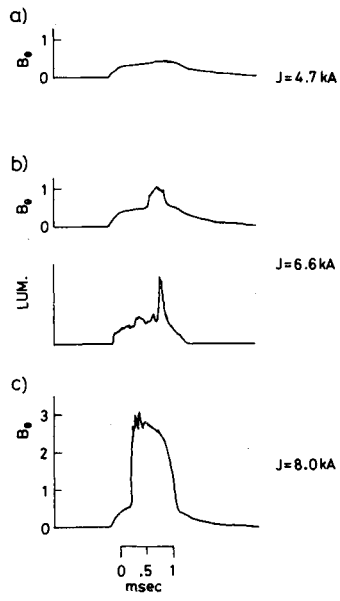

Fig. 11 Magnetic probe signal B_θ. $\dot{m} = 0.12$ g/s, argon. LUM: luminosity.

potential close to the tank potential. The anode and cathode potentials are plotted in Fig. 10 in absolute values for the cathode potential. The anode potential increases more rapidly with J than the cathode potential at small J. Beyond the critical current the anode potential fluctuates and saturates at large J. The cathode potential increases linearly with J at small J, and exhibits a cubic dependence on J and fluctuates beyond the critical condition. From these results, the anode loss is considered to be dominant at the beginning of rapid increase of the discharge voltage and followed by the mode

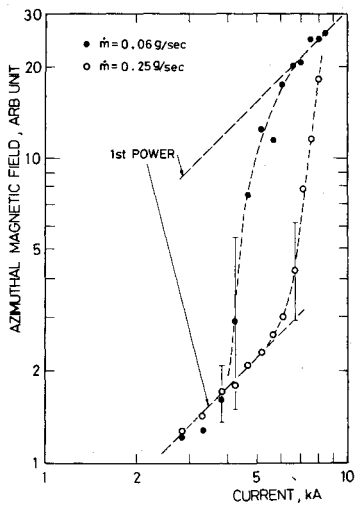

Fig. 12 Variation of azimuthal magnetic field with discharge current, argon.

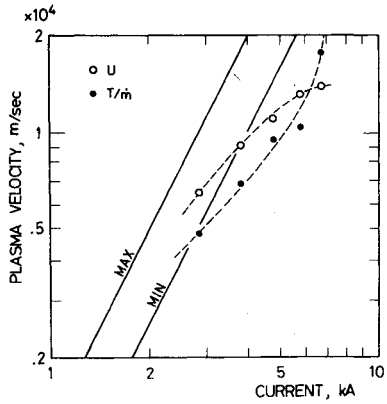

Fig. 13 Plasma velocity measured by directional Langmuir probe, argon. $T/\dot{m}$ is calculated from measured thrust.

change with strong fluctuation. The rapid voltage rise in the supercritical condition is due mainly to the cathode voltage increase and shows the cubic dependence on J, which suggests the electromagnetic acceleration in the cathode region.

V. Diagnostic Measurement

The self-induced magnetic field B_θ was measured by a probe located on the anode surface as shown in Fig. 2a. The probe signals are illustrated in Fig. 11. At small J the B_θ trace is quasisteady, as seen in Fig. 11a. As J increases, the trace shows a bursting irregularity as shown in Fig. 11b. The appearance of the burst almost coincides with that of the voltage fluctuation. This indicates that the discharge current starting from the anode region outside of the radial probe position increases suddenly, and that the discharge current emerges out of the annular region. The plasma luminosity was picked up from the central core of jet by a photomultiplier. The output signal is similar to the B_θ signal as shown in Fig. 11. Since the image covered the central region outside and near the muzzle, the luminosity trace might indicate the gross feature of the change. Taking into account that the major radiation originates from free-free electron-ion collisions, the radiation intensity is proportional to the square of the plasma density. The similarity of the two traces, although not serving as complete proof, suggests that the plasma density is increased outside the arcjet muzzle. This is probably due to the current emerging out of annular electrode region, and the fact that the temporal change of current field is not restricted to a local circumferential anode region but is taking place in the jet core. When J is further increased the B_θ trace becomes quasisteady again, as shown in Fig. 11c. The output of magnetic probe is plotted against J in Fig. 12. At small J, B_θ is proportional to J. This implies that the flowfield of the discharge current is held similar. As the critical condition is

reached, this current pattern is destroyed. By increasing J further, B_θ starts to have a steady value that is much larger than that before the transition. The linear increase of B_θ is plotted in Fig. 7 to be compared with the results obtained by other criteria.

In order to know how the plasma is accelerated, the ion speed was measured by the directional Langmuir probe. For this measurement the ion current was collected by a pair of plane Langmuir probes with surface parallel and perpendicular to the flow and of the same area A_p. Let $J_\parallel$ (parallel) and $J_\perp$ (perpendicular) represent the ion currents collected by the parallel and perpendicular surfaces, respectively. The current $J_\parallel$ is given by

$$J_\parallel = 0.606 e n_i A_p (kT_e/m_i)^{1/2} \tag{9}$$

in thin sheath limit.[14] The ratio $J_\perp/J_\parallel$ is expressed as a function of the ion acoustic Mach number $M = U/(kT_e/m_i)^{1/2}$, where U represents the ion speed.[15]

$$J_\perp/J_\parallel = 1.65M \qquad \text{for } M \geq 1$$

$$J_\perp/J_\parallel = \exp(M^2/2) \qquad \text{for } M \leq 1 \tag{10}$$

This method does not provide sensitive means at $M \ll 1$. Since most of the results in the present experiment were found in the range $M > 1$, this technique might provide reliable results. The ion speed U was measured at 1 m downstream of the arcjet exit. The results were plotted against the current in Fig. 13. The exhaust velocity estimated from the thrust as $T/\dot{m}$ is also plotted in the same figure. The ion speed saturates at large J in contrast to $T/\dot{m}$, which is seen to increase in the current range studied so far. This implies that the ions are not as effectively accelerated as expected from $T/\dot{m}$ results. This may be due to the entrained mass of eroded electrode or insulator.

VI. Conclusions

The following conclusions were obtained in the present experiment. When the arc discharge was forced to be propellant-starved, the anode voltage was increased. This was followed by the discharge mode transition accompanying the strong voltage fluctuation. As the current increased further, the fluctuation was suppressed, and the cathode voltage exhibited the cubic dependence on the discharge current. In this new discharge mode, the electromagnetic acceleration was dominant, but was inefficient possibly due to the occurrence of the mass entrainment at large current.

References

[1] Malliaris, A.C., John, R.R., Garrison, R.L., and Libby, D.R., "Quasi-Steady MPD Propulsion at High Power," NASA CR-111872, 1971.

[2] Jahn, R.G., Clark, K.E., Oberth, R.C., and Turch, P.J., "Acceleration Patterns in Quasi-Steady MPD Arcs," *AIAA Journal*, Vol. 9, Jan. 1971, pp. 167-172.

[3] Hügel, H., "Flow Rate Limitation in the Self-Field Accelerator," AIAA Paper 73-1094, 1973.

[4] Boyle, M.J., Clark, K.E., and Jahn, R.G., "Flow Field Characteristics and Performance Limitation of Quasi-Steady Magnetoplasmadynamic Accelerators," AIAA Paper 75-414, 1975.

[5] Patrick, R.M. and Schneiderman, A.M., "Performance Characteristics of a Magnetic Annular Arc," *AIAA Journal*, Vol. 4, Feb. 1966, pp. 283-290.

[6] Alfvén, H., "Collision between a Non-ionized Gas and a Magnetized Plasma," *Reviews of Modern Physics*, Vol. 32, Oct. 1960, pp. 710-713.

[7] Devillers, P. and Burton, R.L., "The Importance of Alfvén's Critical Velocity for MPD Arcs," AIAA Paper 70-1096, 1970.

[8] Inutake, M. and Kuriki, K., "Fast Ionization Gauge Studies of Quasi-Steady Gas Injection into Vacuum," *Review of Scientific Instruments*, Vol. 43, Nov. 1972, pp. 1670-1674.

[9] Kuriki, K. and Inutake, M., "Establishment of Quasi-Steady Operation in a Pulsed MPD Arcjet," *AIAA Journal*, Vol. 11, Feb. 1973, pp. 133-134; also AIAA Paper 72-496, 1972.

[10] Chen, F.F., "The Leakage Problem in Fusion Reactors," *Scientific American*, Vol. 217, July 1967, pp. 76-88.

[11] Jahn, R.G., *Physics of Electric Propulsion*, McGraw Hill Inc., 1968, Chap. 8.

[12] Clark, K.E. and Jahn, R.G., "Quasi-Steady Plasma Acceleration," *AIAA Journal*, Vol. 8, 1970, pp. 216-220.

[13] Spitzer, L. Jr., *Physics of Fully Ionized Gases*, Interscience Publishers, 1962, Chap. 5.

[14] Bohm, D., Burhop, E.H.S., and Massey, H.S.W., *The Characteristics of Electrical Discharge in Magnetic Fields*, ed. by A. Guthrie and R.K. Wakering, McGraw Hill Inc., 1949, Chap. 2.

[15] Kuriki, K. and Inutake, M., "Super-Alfvenic Flow and Collision Free Shock Wave in a Plasma Wind Tunnel," *The Physics of Fluids*, Vol. 17, Jan. 1974, pp. 92-99.